AFRL-ML-WP-TP-2006-479

MODELING PLASTICITY OF Ni_3Al-BASED $L1_2$ INTERMETALLIC SINGLE CRYSTALS – I. ANOMALOUS TEMPERATURE DEPENDENCE OF THE FLOW BEHAVIOR (PREPRINT)

Y.S. Choi, D.M. Dimiduk, M.D. Uchic, and T.A. Parthasarathy

JULY 2006

Approved for public release; distribution is unlimited.

STINFO COPY

MATERIALS AND MANUFACTURING DIRECTORATE
AIR FORCE RESEARCH LABORATORY
AIR FORCE MATERIEL COMMAND
WRIGHT-PATTERSON AIR FORCE BASE, OH 45433-7750

REPORT DOCUMENTATION PAGE

Form Approved
OMB No. 0704-0188

1. REPORT DATE *(DD-MM-YY)*	2. REPORT TYPE	3. DATES COVERED *(From - To)*
July 2006	Journal Article Preprint	N/A

4. TITLE AND SUBTITLE

MODELING PLASTICITY OF Ni_3Al-BASED $L1_2$ INTERMETALLIC SINGLE CRYSTALS – I. ANOMALOUS TEMPERATURE DEPENDENCE OF THE FLOW BEHAVIOR (PREPRINT)

5a. CONTRACT NUMBER
FA8650-04-D-5233

5b. GRANT NUMBER

5c. PROGRAM ELEMENT NUMBER
61102F

6. AUTHOR(S)

Y.S. Choi and T.A. Parthasarathy (UES, Inc.)
D.M. Dimiduk and M.D. Uchic (AFRL/MLLMD)

5d. PROJECT NUMBER
2311

5e. TASK NUMBER
00

5f. WORK UNIT NUMBER
02

7. PERFORMING ORGANIZATION NAME(S) AND ADDRESS(ES)

UES, Inc.
4401 Dayton-Xenia Rd.
Dayton, OH 45432-1894

Metals Development Team, Metals Branch (AFRL/MLLMD)
Metals, Ceramics, and Nondestructive Evaluation Division
Materials and Manufacturing Directorate
Air Force Research Laboratory, Air Force Materiel Command
Wright-Patterson Air Force Base, OH 45433-7750

8. PERFORMING ORGANIZATION REPORT NUMBER

9. SPONSORING/MONITORING AGENCY NAME(S) AND ADDRESS(ES)

Materials and Manufacturing Directorate
Air Force Research Laboratory
Air Force Materiel Command
Wright-Patterson AFB, OH 45433-7750

10. SPONSORING/MONITORING AGENCY ACRONYM(S)
AFRL-ML-WP

11. SPONSORING/MONITORING AGENCY REPORT NUMBER(S)
AFRL-ML-WP-TP-2006-479

12. DISTRIBUTION/AVAILABILITY STATEMENT

Approved for public release; distribution is unlimited.

13. SUPPLEMENTARY NOTES

The U.S. Government is joint author of this work and has the right to use, modify, reproduce, release, perform, display, or disclose the work.

Journal article submitted to Philosophical Magazine, published by Taylor and Francis.

PAO Case Number: AFRL/WS 06-1845, 28 Jul 2006. Paper contains color.

14. ABSTRACT

A comprehensive mechanism-based crystallographic constitutive model has been developed for L 12-structured Ni_3Al-based intermetallic single crystals. This model represents the unusual thermo-mechanical behaviors of Ni_3Al, such as the anomalous temperature dependence of both the flow stress and strain-hardening rate (SHR), the strain dependence of these anomalous behaviors, and an orientation-dependent tension-compression asymmetry. The model framework was based on two major contributions to plastic flow, namely the repeated cross-slip exhaustion and athermal defeat of screw-character dislocations, and the motion of the macro-kinks (MKs). The contribution of irreversible obstacle storage was incorporated into the constitutive formulations as a resistance against the glide of MKs. The model was implemented in a finite element method numerical framework, and the simulation results showed qualitative agreement with experimental observations.

15. SUBJECT TERMS

Ni_3Al; Ll2 intermetallics; constitutive model; yield anomaly; Kear-Wilsdorf lock; macro-kink

16. SECURITY CLASSIFICATION OF:			17. LIMITATION OF ABSTRACT:	18. NUMBER OF PAGES	19a. NAME OF RESPONSIBLE PERSON (Monitor)
a. REPORT	b. ABSTRACT	c. THIS PAGE			Dennis M. Dimiduk
Unclassified	Unclassified	Unclassified	SAR	60	19b. TELEPHONE NUMBER *(Include Area Code)* N/A

Standard Form 298 (Rev. 8-98)
Prescribed by ANSI Std. Z39-18

Modeling Plasticity of Ni_3Al-Based $L1_2$ Intermetallic Single Crystals - I. Anomalous Temperature Dependence of the Flow Behaviour[†]

Y. S. CHOI *[,2], D. M. DIMIDUK [1], M. D. UCHIC [1] and T. A. PARTHASARATHY [2]

[1] Air Force Research Laboratory, AFRL/MLLM, 2230 Tenth Street, Wright-Patterson AFB, OH 45433-7817, USA

[2] UES, Inc. 4401 Dayton-Xenia Rd., Dayton, OH 45432-1894, USA

* Corresponding Author. Tel.: +1-937-656-7145; fax: +1-937-429-5413

E-mail addresses: Yoon-Suk.Choi@wpafb.af.mil (Y.S. Choi), Dennis.Dimiduk@wpafb.af.mil (D.M. Dimiduk), Michael.Uchic@wpafb.af.mil (M.D. Uchic), Triplicane.Parthasarathy@wpafb.af.mil (T.A. Parthasarathy).

[†] This paper is dedicated to Dr. Peter M. Hazzledine (1940 - 2005), one of few pioneers who brought a unique dislocation behaviour of $L1_2$ intermetallics into the scientific attention.

Abstract

A comprehensive mechanism-based crystallographic constitutive model has been developed for $L1_2$-structured Ni_3Al-based intermetallic single crystals. This model represents the unusual thermo-mechanical behaviours of Ni_3Al, such as the anomalous temperature dependence of both the flow stress and strain-hardening rate (SHR), the strain dependence of these anomalous behaviours, and an orientation-dependent tension-compression asymmetry. The model framework was based on two major contributions to plastic flow, namely the repeated cross-slip exhaustion and athermal defeat of screw-character dislocations, and the motion of macro-kinks (MKs). The contribution of irreversible obstacle storage was incorporated into the constitutive formulations as a resistance against the glide of MKs. The model was implemented in a finite element method numerical framework, and the simulation results showed qualitative agreement with experimental observations.

Keywords: Ni_3Al; $L1_2$ intermetallics; Constitutive model; Yield anomaly; Kear-Wilsdorf lock; Macro-kink

1. Introduction

The most striking feature of Ni_3Al-based ($L1_2$) intermetallic single crystals is their positive temperature dependence of the flow stress over a range of temperature, typically from 200 K ~ 300 K to 600 K ~ 1000 K, which is dependent on a number of factors including alloy chemistry and the crystallographic loading direction. In particular, it is remarkable that this and other anomalous mechanical properties are merely the byproducts of the unique behaviour of the superlattice dislocations. Experimental studies have determined that the screw-character superdislocations readily cross-slip from the {111} octahedral plane to the {010} cubic plane, where their complete core never rests on the cubic plane [1,2]. This results in the immobilization of screw-character dislocations by forming so-called Kear Wilsdorf locks (KWLs) [3,4]. Such unusual dislocation behaviours are responsible for a host of anomalous thermo-mechanical properties, including the positive temperature dependence of the flow stress and the strain-hardening rate (SHR), the offset-strain dependence of these quantities, an orientation-dependent tension-compression (T-C) asymmetry, unusually high SHRs in the micro-strain regime, a partially-to-fully reversible flow behaviour during successive two-step (T_1 and T_2) deformation sequences, and a relatively low strain-rate sensitivity and its temperature dependence.

There have been significant efforts over the past few decades to clarify the micro-mechanisms responsible for these anomalous thermo-mechanical features, and various mechanistic models have been proposed based upon this body of research. Throughout the 70's and mid 80's, much effort was focused on predicting the flow-stress anomaly using models that examined the processes of KWL formation. Takeuchi and Kuramoto (TK) initially proposed a cross-slip-pinning point-obstacle model in order to explain the temperature and orientation dependence of

the yield stress for Ni_3Ga, which is also an $L1_2$ intermetallic [5]. Lall, Chin and Pope modified the TK model to incorporate the influence of the non-Schmid behaviour to the yield stress [6]. Paidar, Pope and Vitek (PPV) derived the activation enthalpy for octahedral-to-cubic cross-slip, which incorporates the anti-phase boundary (APB) energy and resolved shear stresses (RSSs) on octahedral- and cubic-slip systems. This model demonstrated that a T-C asymmetry and its orientation dependence arise from differences in the sign and magnitude of RSS for the constriction of the leading Shockley superpartial before and after the cross-slip event [7]. Yoo extended the models for the driving force for cross-slip pinning by incorporating the elastic interaction torque between superpartial dislocations [8]. Thus, by 1986 all of the essential elements of cross-slip locking (KWL formation) were understood, but these findings were not yet reconciled with TEM observations of dislocation structures, and a reasonable model of slip propagation in the presence of such a potent dislocation locking mechanism did not yet exist.

From the late 80's to mid-90's, considerable advancements were made through developing analytical models that linked the anomalous flow behaviour to more-realistic dislocation glide processes. One model for slip propagation was based on the microscopy studies of Mills et al. [9] and Sun et al. [10], which is called the macro- or super-kink model (MK). In this model, a distribution of edge-character kinks is primarily responsible for dislocation motion through the lateral sweeping of these segments along the mostly-KWL screw-character dislocation lines. Couret et al. [43] measured that MK distribution has an exponential form, and that was later verified by Shi [52]. Hirsch proposed a MK bypass model and derived a corresponding strain-rate formulation that involves activation enthalpies for locking and unlocking KWL configurations [11,12]. Ezz and Hirsch extensively investigated the strain-rate dependence of the flow stress, the strain-hardening behaviour and the two-step (two temperatures T_1 and T_2)

deformation behaviour of $Ni_3(Al,H_f)B$, proposing a flow-stress expression that consists of two (or three) contributions [13-15]. A different model for slip propagation was proposed by Caillard, who interpreted the yield-stress and SHR anomalies as resulting from the temperature-dependent 'exhaustion' of mobile dislocations through the formation and defeat of KWLs [16]. Based on this interpretation, he proposed an exhaustion-hardening model for plastic flow at small strains [16]. Louchet proposed a different model, called the 'extended locking-unzipping' (ELU) model [17], where the strain-rate sensitivity and the flow stress anomaly were expressed as a function of the dislocation exhaustion and multiplication rates, which in turn were dependent on the temperature-dependent distribution of mobile MKs.

In addition to analytical modeling, discrete dislocation-dynamics (DD) simulations have also helped to identify the source of plastic flow at either the single dislocation or dislocation-ensemble scale. Mills and Chrzan first performed 2-D DD simulations of individual dislocation motion using a point-pinning criterion for an expanding dislocation loop, where the probability of pinning was dependent upon the local orientation of the dislocation line [18]. The dislocation configurations resulting from their DD simulations were somewhat consistent with experimental observations and, suggested that the primary consequence of local cross-slip pinning is the self-exhaustion of mobile dislocations. More advanced DD simulations (2-D) were performed by Devincre and Veyssière et al. for two different simulation configurations [19,20]. The first was an 'in-plane' configuration similar to the Mills-Chrzan simulations. This simulation showed that MK motion is the dominant source of plastic flow at low temperatures in the anomalous flow regime, which is strongly influenced by the mobility of cross-slip jogs (CJs) on the cubic planes. The second type of simulation examined small ensembles of screw-character dislocations using an 'end-on' configuration, which allowed cross-slip (KWL formation) of screw-character

dislocations between octahedral and cubic planes, but did not account for the glide (or multiplication) of MKs [20]. Based on examination of the SHRs and the evolution of the KWL-height distribution from these 'end-on' simulations, they concluded that large SHRs in the anomalous temperature regime stem from "*the preferential exhaustion of the weakest locks and to some extent the shape of their distribution*" [20]. However, the positive temperature dependence of SHR was not observed in their 'end-on' DD simulations.

In contrast to the extensive dislocation-level modeling of these materials, only a few attempts have been made to develop a crystallographic constitutive model for $L1_2$ alloys. Unfortunately, nearly all of these are rooted in the early concepts of point pinning. Qin and Bassani developed a yield function that incorporated the non-Schmid yield behaviour of $L1_2$ alloys [21]. The basic structure of their yield function originated from the mechanistic model for cross-slip activation enthalpy proposed by PPV [7]. They placed this yield function within the framework of a 'rate-independent' constitutive law, and successfully simulated the T-C asymmetry behaviour of $L1_2$ alloys [22]. Cuitino and Ortiz developed a more elaborate constitutive model [23], where strain hardening for octahedral slip consisted of a contribution from both random forest obstacles and cross-slip pinning. The obstacle-generation rate was proportional to the rate of cross-slip pinning, and the rate of cross-slip pinning was expressed using the PPV model [7]. Bassani [24] pointed out a physical inconsistency of their model in that they used a point-pinning-obstacle-based hardening model incorporating non-Schmid effects, while the driving force for slip followed the Schmid stress. Allan utilized an expression similar to that of Cuitino and Ortiz in order to determine the obstacle density due to cross-slip pinning [25]. Kameda and Zikry proposed a constitutive model that involves separate evolution equations for mobile and immobile dislocation densities [26]. Both evolution equations also incorporated the rate of cross-slip

pinning using the PPV activation enthalpy [7]. Most of these constitutive models incorporated strain-hardening descriptions via point-obstacle pinning, which is inconsistent with the current models of slip processes and the physical evidence that supports them. Recently, new efforts were made for constitutive modeling such that the whole mechanistic event was accounted for as delocalized locking under a dislocation loop-expansion configuration. This approach was motivated by modern understanding of dislocation mechanisms for Ni_3Al-based intermetallics. Yuan and Parks [27] developed a constitutive model based upon Hirsch's MK-bypassing model [11] and Caillard's self-unlocking model [36]. Finally, the present authors also proposed a constitutive model that utilized the concepts of exhaustion hardening suggested by Caillard [16] and flow-stress partitioning proposed by Ezz and Hirsch [13-15], which qualitatively represented both the anomalous yield stress and SHR behaviours [28].

The present study is aimed at developing a comprehensive constitutive model that encompasses all of the major thermo-mechanical features of Ni_3Al-based single crystals; but, one that is also based on experimentally-observed dislocation behaviours and the corresponding insights into mechanisms that they provide. The model presented here differs from the previous study [28], which was not able to accurately represent thermally-reversible flow as observed in Cottrell-Stokes (C-S) two-step deformation experiments. In the present study, the constitutive model has been completely restructured by incorporating two major contributions to plastic flow—MK glide and the athermal defeat of incomplete KWL—that occur during dislocation-loop expansion. The new model was used to simulate the thermally reversible flow behaviour for C-S type two-step deformation, and the results are presented in a subsequent paper [59]. Since the 'microscopic' dislocation behaviours for this class of alloys are at least as complicated as many of their 'macroscopic' thermo-mechanical features, this paper starts with identification and discussion of

the fundamental issues affecting $L1_2$ alloy flow behaviour. Additionally, our interpretation of these issues is presented within the context of developing the new constitutive descriptions. Finally, simulation results from the new constitutive model are presented and the physical implications of these findings are discussed.

2. The dislocation behaviour in $L1_2$ alloys

Identifying the dislocation mechanisms responsible for plastic flow is probably the most debated issue in understanding the deformation behaviour of Ni_3Al-based single crystals. There is general agreement that the mobile dislocation density is repeatedly and progressively exhausted due to the formation of KWLs in the small strain regime (typically less than 1% strain). An increase in the applied stress is required to re-mobilize these locked dislocation configurations, which eventually gives rise to a high SHR [16,20,29]. Due to the dominance of the KWL formation, the dislocation configurations consist of long, straight screw-character dislocations that are three-dimensionally connected by CJs on the cubic planes and MKs in a series of parallel octahedral planes (see [30] for a comprehensive review). Here, one needs to understand how plastic strain can proceed from this common dislocation origin.

Hirsh's work emphasized the contribution from bypassing (hence unlocking) of KWLs by wrapping-around MKs through a thermally activated process [11,12]. Ezz and Hirsch corrected Hirsch's original model by incorporating an 'athermal' MK process [13,14]. Their model suggested that the major source of mobile dislocations for plastic flow is from the operation of MK-based Frank-Read (FR) sources. These sources were described as having an initial critical configuration which derived from the combination of repeated cross-slip locking of screw-

character dislocations as well as the interactions of moving edge- (or near-edge) character dislocations with obstacles, both as integral parts of dislocation loop expansion (see Fig. 11 in [14] for details). However, their model did not explain the source for plastic flow in the microstrain regime (typically less than 0.5% strain) [29], nor did it quantitatively explain the thermally-reversible nature of the yield stress [15].

Alternatively, Caillard proposed an exhaustion-hardening model by which the plastic strain proceeds through athermal cross-slip unlocking of KWLs [16,31]. The issue of complete dislocation loop expansion was not quantitatively treated in this model. Thus, Devincre and Veyssière et al. [19] criticized Caillard's model because they had previously observed that MK motion contributed significantly to the total plastic strain for their 2-D 'in-plane' DD simulations. However, the yield-stress anomaly predicted from their 'in-plane' DD simulations was found to be comparable with the one predicted from their later 'end-on' DD simulations (see Fig. 3 in [20] for details), which did not incorporate MK glide. This seems to imply that screw-character dislocation glide, which is accomplished by either athermal unlocking of KWLs or MK glide, leads to almost equivalent stress-strain responses in the microstrain regime. It is also possible that models are equivalent only to the degree that they have been represented in simulation.

Caillard later extended his theory after investigating the difference between the peak temperatures for yield stresses and those for SHRs ($T_P(\tau_{max})$ and $T_P(\theta_{max})$, respectively). It is generally observed that $T_P(\theta_{max})$ is lower than $T_P(\tau_{max})$ by a few hundred degrees Centigrade, depending upon the alloy stoichiometry and the loading direction [13,32,33]. Caillard proposed that the occurrence of $T_P(\theta_{max})$ is closely related to the onset of athermal unlocking of incomplete KWLs,

for which the cross-slip distance (w) in the cubic plane (i.e. the CJ height) is about the magnitude of a Burgers vector b [34,35]. The threshold stress, τ_i, for this unlocking was expressed by

$$\tau_i = \frac{\Gamma_{111}}{b}\left(1 - \frac{\Gamma_{100}}{\Gamma_{111}}\frac{1+2/A}{\sqrt{3}}\right), \quad (1)$$

where Γ_{111} and Γ_{100} are APB energies in the octahedral and cubic planes, respectively, and A is the elastic anisotropy factor ($2C_{44}/(C_{11}-C_{12})$, where C_{ij} are the elastic constants). Experimental results showed that the stress $\tau(\theta_{max})$ corresponding to the maximum SHR for different types of Ni_3Al-based alloys reasonably follows a linear relationship with Γ_{111} ($\tau(\theta_{max}) = (0.24/b)\cdot\Gamma_{111}$), which is equivalent to equation (1) when A and $\Gamma_{100}/\Gamma_{111}$ are approximated to be 3.3 and 0.8, respectively [34,35]. Note that these values reasonably represent the experimental measurements [7,8,37]. This result strongly supports the relationship between the SHR peak and the initiation of unlocking of incomplete KWLs.

The contribution (if any) of cubic slip to anomalous plastic flow is perhaps the least known contribution. It is generally believed that the monotonic stress decrease above $T_P(\tau_{max})$ is related to significant levels of slip on the cubic planes [5]. However, the dislocation behaviour on the cubic plane, particularly the CJ behaviour in the anomalous temperature regime, is virtually unknown. Ezz, Sun and Hirsch suggested that a SHR decrease after $T_P(\theta_{max})$ is ascribed to the increased mobility of CJs [29,32]. Based on the results from 'in-plane' DD simulations, Devincre and Veyssière et al. concluded that a yield-stress anomaly can be captured only when the mobility of CJs is restricted in order to control the free glide of MKs [19]. A similar suggestion was also previously made by Dimiduk [58]. Conforto, Molénat and Caillard suggested that screw-character dislocations can glide substantial distances in the cubic plane for $L1_2$ intermetallics having high complex stacking fault (CSF) energies because of a reduced dissociation width for

the superpartial dislocations on the octahedral planes [37]. However, they also suggested that the mobility of near-edge segments on the cubic plane is restricted by strong local pinning [37]. Note that no mechanistic model has been proposed for the gliding behaviour of CJs, especially as a function of their height and the deformation temperature. Yet, such information is ultimately necessary for quantitative results in all of the models

From the discussion to this point, one may notice that the prior models suggest that the plastic strain can proceed by two major contributions, either by screw-character dislocation glide through the repeated locking-athermal unlocking process, and/or by MK glide on the octahedral planes. Strictly speaking, these two processes are not mutually separable because once a critical-height MK propagates, a new set of locked screw-character dislocations (along with a new set of MKs) is generated from this event. Likewise, athermal unlocking of KWL segments may lead to curved dislocations that behave like mobile MKs in bulk samples. However, it is often argued that one micro-mechanism dominates over the other for separate ranges of temperature (or stress). For example, under a circumstance that all screw-character dislocations are exhausted by forming KWLs, but at a stress still too low to allow athermal defeat, plastic flow likely depends upon MK motions in the octahedral plane to sustain a mobile dislocation density. This situation can apply to the low-temperature (i.e. low stress) domain of the anomalous regime, especially for high CSF-energy alloys. For conditions when the stress is high enough to athermally unlock KWLs, the re-mobilized screw-character dislocations will dominate the mobile dislocation density and contribute to plastic flow. This ‘bifurcated’ approach was already suggested by Caillard [34,35], Devincre and Veyssière et al. [19,20], and Hirsch and Ezz [29,32], although slightly different interpretations were made by each of them. It is also important to note that every model of anomalous flow that has been introduced since the early 90’s, together with virtually all of the

experimental data, support the notion of delocalized KW locking rather than point-pinning obstacles. However, this physical feature has only been recently incorporated into constitutive models [27,28].

3. Structuring constitutive descriptions

The construction of a new constitutive model begins with the incorporation of the two major dislocation glide processes (MK motion and screw dislocation glide after the athermal defeat of KWLs) into corresponding constitutive formulations. A framework for the strain-rate description was developed from the following simple dislocation configuration. Suppose that a dislocation having a line length l in a given volume V travels a distance λ on a slip plane. The plastic shear strain produced by this event can be expressed by $\gamma = b(A/V)$, where A is the area ($l \cdot \lambda$) swept by a dislocation. The time derivative of this expression provides the resulting strain rate, $\dot{\gamma} = b(\dot{A}/V)$. Now, consider a simple rectangular dislocation loop ($l_e \times l_s$) that expands outwards with velocities v_e and v_s for edge and screw-character dislocations, respectively. The time rate of the increment of the area swept by a dislocation loop can be written by $\dot{A} = 2(l_e v_e + l_s v_s)$. Here, this expression assumes that pairs of edge- (or screw-) character dislocations glide in opposite directions with a uniform velocity v_e (or v_s for screw-character dislocation), hence the factor 2. Coupling the two rate expressions yields

$$\dot{\gamma} = b\rho_e v_e + b\rho_s v_s, \qquad (2)$$

where ρ_e and ρ_s are dislocation densities for edge- and screw-character dislocations, respectively. Equation (2) represents an Orowan [38] relation generalized for edge- and screw-character dislocations, which is often used both for a framework of constitutive descriptions [39,40] and for dislocation modeling [41].

In the present constitutive model, the behaviours of edge- and screw-character dislocations ($\rho_e v_e$ and $\rho_s v_s$, respectively) in equation (2) were linked to those for MKs and KWLs, respectively. The edge-character dislocations were assumed to follow the kinetics of the MK glide, and the screw-character dislocations were assumed to be dictated by the model of locking/unlocking KWLs. This assumption may not be entirely satisfactory. However, it offers a significant improvement over prior models in terms of being comprehensive, and captures all important attributes of Ni_3Al's thermo-mechanical behaviour. Even though the configuration of a dislocation loop for Ni_3Al-based single crystals is distinguishable from that for ordinary FCC crystals, we believe that the generalized Orowan description is still applicable to MKs and KWLs if both edge- and screw-character dislocation behaviours are fully described by MK and KWL behaviours, respectively[‡]. Toward this end, equation (2) may be rewritten as

$$\dot{\gamma} = b\rho_{mK} v_K + b\rho_{mw} v_w . \qquad (3)$$

In equation (3), ρ_{mK} and ρ_{mw} are the mobile dislocation densities tied to MK motion, and repeated locking and athermal unlocking of KWLs, respectively, and v_K and v_w are the corresponding average dislocation velocities for these segments, where the subscript *w* indicates the cross-slip distance in the cubic slip plane by the screw-character dislocation. In the subsequent subsections we describe how these are linked to the physical dislocation structures.

3.1 Descriptions for ρ_{mK} and v_K

[‡] Note that Ni_3Al-based single crystals have a three-dimensional dislocation configuration for which both locked screw-character dislocations (KWLs) and edge- or near-edge character dislocations (MKs) reside on different but parallel octahedral planes. These dislocation segments are linked by CJs of various heights on cubic planes. However, since the regime of the yield-stress anomaly is dominated by octahedral glide and, since the kinetics of the CJs are completely unknown, this model approximates the real behaviour through 2D planar loop expansion and variations in segment velocities that essentially represent the effects of the CJs.

The present model links the quantity ρ_{mK} to the MK-height distribution. The experimentally measured probability distribution function (PDF), $P(h)$, of MK heights, h, at steady state is known to follow an empirical relation [42,43];

$$P(h) = P_o \exp\left(-\frac{h}{\bar{h}}\right), \quad (4)$$

where P_o and $\bar{h}$ are the pre-exponential normalization constant and the average MK height, respectively. Since $\bar{h}$ tends to evolve with strain and temperature, $P(h)$ also depends upon those parameters. During straining, the current stress mobilizes some portion of the MK population and this can be linked to ρ_{mK}. Referring back to equation (3), we express ρ_{mK} by

$$\rho_{mK} = \rho_{Ktot} \cdot f_{mK}(\gamma, T). \quad (5)$$

This equation states that the mobile density of MKs (ρ_{mK}) is the total MK density (ρ_{Ktot}) multiplied by a fraction of those mobilized (f_{mK}) for a given temperature and the cumulative strain. Here, ρ_{Ktot} represents all edge- or near-edge character dislocations in the octahedral planes. It is difficult to determine the evolution and the temperature dependence of ρ_{Ktot}. In the small strain range (typically less than about 3% strain) the evolution of ρ_{Ktot} is expected to be almost negligible relative to some starting state. Unfortunately, no experimental data are available for the estimation of $\rho_{Ktot}(\gamma,T)$.

The fraction of mobile MKs is simply that fraction which has MK heights above a critical value, which depends on the resolved stress. Accordingly, in equation (5), f_{mK} was determined using the following expression;

$$f_{mK} = \frac{\int_{h_c}^{\infty} P(h)dh}{\int_{o}^{\infty} P(h)dh} = \exp\left(-\frac{h_c}{\bar{h}}\right), \quad (6)$$

where h_c is the critical MK height, above which MKs are mobilized by bowing out. Louchet utilized a similar expression in his 'ELU' model [17]. By writing equation (6) MKs are assumed to have distribution $P(h)$ upon plastic straining, and those having heights larger than h_c are mobilized, where the fraction mobilized is linked to the mobile dislocation density. It now remains to describe the strain-dependent evolution and temperature dependence of h_c and $\bar{h}$. We expect these parameters to gradually decrease with increasing strain (i.e. increasing stress), thus shifting the PDF curve $P(h)$ to the left: but the detailed evolution behaviour has not been reported and is *a priori* unknown. We assumed that both parameters start from some initial values (h_{co} and $\bar{h}_o$) and evolve towards final saturation values (h_{cs} and $\bar{h}_s$). Further, as both of the parameters eventually evolve from strain hardening, we assume that they decay asymptotically between these two limits during plastic straining. Accordingly, we assume the following formalism for the evolution between the two bounds;

$$\frac{dh_c}{d\gamma} = -\theta_{hc}\left(\frac{h_c - h_{cs}}{h_{co} - h_{cs}}\right) \text{ and} \quad (7)$$

$$\frac{d\bar{h}}{d\gamma} = -\theta_{\bar{h}}\left(\frac{\bar{h} - \bar{h}_s}{\bar{h}_o - \bar{h}_s}\right), \quad (8)$$

where θ_{hc} and $\theta_{\bar{h}}$ are initial decay rates for h_c and $\bar{h}$, respectively. We believe that the asymptotic evolution toward a saturation limit is a common phenomenological nature of major physical (or mechanical) quantities involved in dislocation-based crystal plasticity. One notices from equations (7) and (8) that the evolution of h_c and $\bar{h}$ depends upon the initial decay rate (θ_{hc} and $\theta_{\bar{h}}$) and the decay range ((h_{co}–h_{cs}) and $(\bar{h}_o - \bar{h}_s)$). The initial and saturation values of h_c in

equation (7) were determined by the following expressions that tie them to the physical stress acting on dislocation sources;

$$h_{co}(T) = \frac{\alpha\mu(T)b}{\tau_o(T)} \text{ and} \tag{9}$$

$$h_{cs}(T) = \frac{\alpha\mu(T)b}{\tau_i(T)}, \tag{10}$$

where α, μ and τ_o are the geometric parameter in a Taylor-type relation, the shear modulus (temperature dependent) and the CRSS in the octahedral plane at the onset of plastic slip, respectively. At saturation, the stress corresponding to h_{cs} was tied to τ_i of equation (1) that sets a lower limit of the activated MK height through the stress for athermal KWL defeat. Such a limit basically assumes that the contribution of MK glide is only significant in the regime prior to the onset of athermal breakaway of incomplete KWLs.

From equations (9) and (10) the temperature dependence of h_c was incorporated through the temperature dependence of μ, τ_o and τ_i. In equation (8) an initial value of the mean MK height ($\bar{h}_o$) was determined, based on a relation that $\bar{h}$ is inversely proportional to the probability of cross-slip locking [20,30];

$$\bar{h}_o(T) = c_f \exp\left(\frac{k_d G_{KPo}}{kT}\right), \tag{11}$$

where G_{KPo} is the activation energy for cross-slip (G_{KP}) [16] (by a kink-pair mechanism [44]) at the onset of plastic slip, and k and c_f are the Boltzmann's constant and the proportionality constant, respectively. The parameter k_d is a damping constant that is introduced to obtain better fit with experimental results, while retaining all the physics contained in prior derivations of G_{KPo}. A more detailed discussion of k_d is given later. In equation (11) G_{KP} is given by [16]

$$G_{KP} = 2U_c + Kb^3\left[2\sqrt{2\alpha' r} - \sqrt{\frac{\tau_{cs}}{2\pi K}}\right], \tag{12}$$

where K, α' and r are the energy factor (= $[0.5C_{44}(C_{11}\text{-}C_{12})]^{1/2}$), the geometric factor for line tension and the recombination-energy factor, respectively. In equation (12) τ_{CS} and U_c are the stress projected on the cubic plane in the slip direction [45] and the constriction energy for the superpartial dislocation (PPV model [7]), respectively. These terms are given by

$$\tau_{CS} = \frac{\Gamma_{111}}{b}\left[\frac{A\sqrt{3}}{A+2} - \frac{\Gamma_{100}}{\Gamma_{111}}\right] + \tau_{cb} \text{ and} \tag{13}$$

$$U_c = \frac{\mu b^3}{4\pi}h' + \frac{\mu b^3}{4\pi}\kappa'\frac{b}{\Gamma_{111}}\left[\tau_{pe} - \kappa\tau_{se}\right]\frac{\Gamma_{111}}{\Gamma_{CSF}}, \tag{14}$$

where τ_{pe} and τ_{se} are the resolved shear stresses for the primary and the secondary octahedral slip systems, respectively, and τ_{cb} is the resolve shear stress on a corresponding cubic slip system. One can find a list of primary and secondary slip systems for τ_{pe} and τ_{se} and the corresponding cubic slip system for τ_{cb} in [21] and [25]. In equation (14), h' is a non-dimensional constant, and κ' and κ are the parameters that determine the relative magnitude of a T-C asymmetry and the orientations for which the T-C asymmetry vanishes in a stereographic triangle, respectively. Unfortunately, despite the physical basis for the derivation of these expressions, the magnitude of the theoretical activation energy (G_{KPo}) as determined from equations (12) through (14) usually produces an unusually high temperature dependence of $\bar{h}_o$ through equation (11) compared with experimental data, which is unacceptable. Thus, we introduced a damping constant k_d in the exponential term of equation (11). Caillard already pointed out this issue [16]. This seems to be related to the large discrepancy between the theoretical value of the activation energy from mechanistic models and the apparent value of the activation energy from experimental yield-anomaly data [14]. The former is based upon equations (12) to (14) that were driven from force

balances on a single-superdislocation configuration *viz.*, a pair of superparitial dislocations, while the latter is based upon the generalized "collective" behaviour of dislocations in a deforming crystal.

The average velocity (v_K) corresponding to ρ_{mK} in equation (5) was expressed in our model by a dislocation-drag based form;

$$v_K = \frac{\tau - \tau_K}{B} b , \qquad (15)$$

where τ, τ_K and B are the applied stress, the resistance (i.e. strength) against MK gliding and the drag coefficient, respectively. Note that a similar form of the velocity description for MKs was also used in DD simulations [19]. To define τ_K, the concepts introduced by Ezz and Hirsch proved useful. In their model the flow stress (τ_{flow}) was partitioned into several contributions [13-15];

$$\tau_{flow} = \tau_p(T) + \tau_h(\gamma, \dot{\gamma}, T) \text{ or } \tau_p(T) + \tau_f(\gamma) + \tau_t(\dot{\gamma}, T) . \qquad (16)$$

In equation (16), τ_p is the temperature-dependent contribution that is primarily responsible for the yield-stress anomaly. This means that it carries a thermally "reversible" part of the flow stress. They set this term to provide a critical configuration for the operation of Frank-Read (FR) sources [14]. The second term τ_h in equation (16) is the contribution from the formation of dislocation forests and obstacles that can be overcome with aid from thermal activation. This term is dependent upon the plastic strain, its rate and temperature. A part of this term is thermally "irreversible", which means that it is stored and persists between steps during two-step (T_1 and T_2) deformation [15]. Partially based on equation (16) τ_K in equation (15) was expressed as

$$\tau_K = \tau_o + \tau_f . \qquad (17)$$

Here, τ_o was already determined by equation (9) and τ_f is our definition of the contribution from forest obstacles. In Ezz and Hirsch's original model, the mechanism for the formation of forest obstacles was described by the multiplication of FR sources and their interactions with cross-slip locking and bypass-unlocking events [14,32]. However, in the present model since the screw- and edge-character dislocations are treated separately, all mechanisms contributing to τ_K, such as dipole debris, antiphase-boundary-tube formation, cubic-plane glide debris, etc., are phenomenologically gathered into this term. These processes are accounted for in a collective phenomenological way by considering them irreversible hardening and, the resulting SHRs from these processes are treated similarly to forest hardening in ordinary metals. Therefore, τ_f was written as an 'ordinary' FCC-like hardening contribution and the carrier of the irreversible part of the flow stress during two-step deformation. The evolution of τ_f was set to follow Voce-type parabolic-hardening law, that is typical for forest hardening;

$$\frac{d\tau_f}{d\gamma} = \theta_f \left(\frac{\tau_{fs} - \tau_f}{\tau_{fs}} \right), \tag{18}$$

where θ_f and τ_{fs} are the initial hardening rate and the saturation value of τ_f, respectively. In equation (18) τ_f is probably almost negligible at the onset of plastic slip for well annealed crystals, but its influence is expected to increase gradually after the initial stage of plastic slip.

3.2 Descriptions for ρ_{mw} and v_w

The previous section described the treatment of the evolution, and strain-rate contribution of edge-character dislocations in the present model (the first term in equation (3)). As mentioned earlier, the flow behaviour of screw-character dislocations was tied to that of locking/unlocking

of KWLs (the second term in equation (3)). We utilized the concept of Caillard's exhaustion-hardening model [16] and the athermal defeat of incomplete KWLs [31,35] in order to describe this behaviour. According to Caillard's model, at the early stage of the plastic deformation (almost at the onset of plastic slip) all screw character dislocations are rapidly and 'effectively' instantaneously exhausted by forming KWLs having various cross-slip distances (w's) from b to mb, where mb is the maximum CJ height allowed. While KWLs are defeated through MK motion, they may also be defeated athermally in the absence of MKs under the sufficient stress. Thus, as the stress (or equivalently the temperature) increases, this athermal breakaway process gives rise to increments of plastic strain and the corresponding SHR. Here, we assumed that the stress required to unlock KWLs of $w=b$ is equivalent to the unlocking stress for incomplete KWLs [34,35], which was given by τ_i in equation (1). Note that Saada and Veyssière made an independent analysis of the KWL-breaking stress that gave different values [57]. This point is not yet reconciled. Caillard's exhaustion hardening can be expressed by

$$\frac{d\tau_w}{d\gamma} = \theta_{10} \exp\left(-\frac{G_{CS}}{kT}\right)\exp\left(-\frac{\tau_w - \tau_i}{\tau_w^* - \tau_i}\right), \tag{19}$$

where τ_w is the strengthening contribution from locking and athermal unlocking of incomplete and complete KWLs, and G_{CS} is the activation energy for cross-slip over distances of $w > b$, which is given by [16]

$$G_{CS} = U_c + K^2 b^3 \left[\frac{4r\sqrt{2\alpha' r}}{3\tau_{cs}}\right]. \tag{20}$$

Here, τ_w* is the stress required to unlock the KWLs having $w = \overline{w} + b$, where $\overline{w}$ is the average w at a given temperature. Also, θ_{10} is the pre-exponential factor. In equation (19) the first and second factors of the RHS are related to the probability of locking for all KWLs having $b < w \leq mb$. The third factor on the RHS in equation (19) corresponds to the fraction of the KWLs that

remain locked under the stress τ_w, where these KWLs correspond to those having $w > w_c$ (w_c is defined in equation (21)). Note that this factor decays exponentially with increasing τ_w. Thus, equation (19) represents the formation and gradual defeat of KWLs with increasing applied stress, independent of MK motion. This results in a change in SHR by controlling the exhaustion rate of the mobile dislocation density.

Formulating ρ_{mw} is a real challenge. No experimental data have been reported for the distribution of cross-slip distances, $N(w)$, even though this distribution was approximated as a Gaussian form in the DD simulations done by Devincre and Veyssière et al. [20]. Similar to equation (6) it can be roughly estimated by

$$\rho_{mw} \propto \frac{\int_0^{w_c} N(w)dw}{\int_0^{\infty} N(w)dw}, \tag{21}$$

where $N(w)$ and w_c are the PDF of w and the critical height below which KWLs ($w \leq cb$) are athermally defeated, respectively. According to the results of DD simulations by Devincre and Veyssière et al. [20], as the strain (or the temperature) increases, both $N(w)$ and w_c tended to shift toward the higher w range. We interpreted this behaviour as a relatively constant value of ρ_{mw} during plastic deformation, which leads to the approximation of $d\rho_{mw}/d\gamma \approx 0$. This can be understood in a physical sense by defining the nature of screw-character dislocation locking and defeat (and the associated length scales) as insensitive to the prior deformation history.

During plastic deformation, the KWLs remain locked until the driving stress becomes high enough to athermally break the locks. Once unlocking occurs, the dislocations travel short distances in the octahedral plane until they cross-slip again forming new KWLs. This athermal breakaway-relocking process is repeated throughout the plastic deformation and consequently

contributes to plastic flow. The process also sets a limit on stress and the SHR. This behaviour is phenomenologically comparable to the 'stop-and-go' jerky glide behaviour of ordinary FCC metals [46]. Since the latter can be expressed in a form of thermally activated plastic flow proposed by Kocks, Argon and Ashby [46], we also adopted the similar form for the representation of the average velocity v_w corresponding to ρ_{mw};

$$v_w = v_o \exp\left(-\frac{F_o}{kT}\left[1 - \left[\frac{\tau - \tau_A}{\tau_T} \right]^p \right]^q \right), \qquad (22)$$

where p and q are parameters determining the nature of obstacle profiles [46], and v_o and F_o are the free-flight velocity and the total free energy required to overcome short-range obstacles without assistance of external work, respectively. In equation (22), all braces, [ ], were defined such that $[x] \equiv x$ if $x > 0$, otherwise $[x] \equiv 0$, where x is the quantity inside the inner braces. Following the interpretation by Balasubramanian and Anand [47], τ_A and τ_T in equation (22) are the strengthening contributions from the athermal (long-range character) and the thermally-activatable (short-range character) obstacles, respectively.

Even though the current model utilized the generalized form of the jerky-glide behaviour for the representation of the KWL breakaway-relocking behaviour of screw-character dislocations, note that there is a subtle (but still meaningful) difference between these two behaviours. The former is usually represented by the glide-resistance profile in the presence of short-range thermally-defeatable obstacles and long-range athermal obstacles [46,47]. However, it is believed that the glide-resistance profile for the latter is represented mainly by athermal barriers for unlocking of KWLs. The contribution of short-range obstacles is expected to be negligible for this case, because cross-slip locking of screw-character dislocations is so quick that moving (or unlocked)

screw-character dislocations barely have a chance to interact with short-range obstacles prior to their cross-slip relocking.

In this sense, the contribution of τ_A in equation (22) is more significant than that expected from the typical jerky-glide behaviour of FCC metals. Thus, τ_A of equation (22) was replaced with τ_w of equation (19). This is because the nature of cross-slip locking in Ni_3Al-based single crystals is so rapid that it can be modeled as effectively rate-insensitive (for the rates of quasi-static tests). Even though the cross-slip frequency is strongly temperature dependent, locking of screw-character dislocations takes place 'effectively' instantaneously at any given temperature (within the anomalous temperature regime) so that one can view its behaviour as a rate and time-independent stress-controlling process. However, τ_T in equation (22) was considered as an adjustable parameter due to a lack of understanding of the mechanism(s) responsible for τ_T. It is also unclear whether or not this term is related with τ_t in Ezz and Hirsch's framework (equation (16)). The ordinary forest-obstacle contribution τ_f, which was incorporated in the MK strength contribution τ_K in equation (17), was not considered to be associated with τ_T in equation (22). This is because cross-slip locking is believed to dominate over forest obstacles for the exhaustion of screw-character dislocations, as discussed in the previous paragraph. One should notice from equations (19) and (22) that v_w becomes influential only when $\tau > \tau_i$. This means that the contribution of the screw-character dislocations stemming from repeated exhaustion-breakaway of KWLs becomes important upon unlocking of the weakest KWLs (i.e. incomplete KW locks) whose 'onset' stress corresponds to τ_i in equation (1).

3.3 Summary of constitutive descriptions

All constitutive formulations described in Sections 3.1 and 3.2 were rewritten for an individual slip system, *s* and, are summarized in Appendix A. Note that these descriptions are only for the twelve octahedral slip systems (equations (A1) to (A19)). Six cubic-slip systems were also incorporated in the present constitutive model as described by equations (A20) to (A23). However, negligible strain hardening was introduced for the cubic slip systems, such that cubic slip behaves almost perfectly plastic once it is activated. Under the framework of these constitutive descriptions, the flow behaviour of Ni_3Al-based intermetallic single crystals can be qualitatively described as follows.

Upon plastic straining the screw-character dislocations are 'effectively' instantaneously exhausted by forming KWLs, and almost simultaneously the dislocation-loop configurations are filled with various heights of MKs and CJs that link locked screw-character dislocations. The distribution of MK heights is expressed by $P(h)$, and this distribution is set by the locking behaviour of screw-character dislocations because the initial geometry of $\bar{h}$ ($\bar{h}_o$) is determined by G_{KPo} through equations (A11) and (A13). Those equations in turn are based on the balance of forces acting on the screw-character dislocations (U_c^s and τ_{CS}^s from equations (A14) and (A15)) controlling cross-slip. The temperature dependence of $P(h)$ also enters in a similar way through equations (A9) to (A11). Formation of such loop configurations is consistent with a widely accepted understanding for anomalous flow suggesting that the lack of mobile dislocation density (i.e. rapid exhaustion of mobile dislocations) is responsible for the high SHR and the diffuse elastic-plastic transition in the micro-strain regime. Here, the progress of plastic flow (hence the flow stress and SHR) explicitly depends upon the availability of the mobile dislocations from kink motion ($\rho_{mK} v_K$) or from athermal unlocking of KWLs ($\rho_{mw} v_w$). This means that plastic flow is source-controlled in this regime.

While both MK motion and athermal unlocking lead to source-controlled flow, the nature of how each mechanism contributes to plastic flow has a different interpretation in the present model. For the former, evolution of ρ_{mK} (equation (A5)) was controlled by evolution of h_c and $\bar{h}$ (equations (A7) and (A8)), which means that the source for ρ_{mK} is controlled by the activation of the "weak" (large) MKs. This was represented by the fraction of the mobilized MKs through equations (A5) and (A6). Once MKs are mobilized, these dislocation segments glide at an average velocity v_K. This velocity is dislocation-drag based and relatively high. In DD simulations [19,20] mobilized MKs travel at this high velocity, and glide is quickly stopped either by encountering other obstacles or by cross-slip locking of screw segments that were generated from MK motion. The same concept was applied to the current model. The MK velocity was set to be controlled by the glide resistance due to forest obstacles through τ_f in equations (A3) and (A2). Since the cross-slip locking was considered as a rapid event, this also implicitly accounts for quick immobilization of screw segments generated from MK gliding. For the screw-character glide processes, we focused on two concepts: the quick 'effectively athermal' nature of the KWL formation, and the resultant jerky glide motion due to the repeated breakaway and subsequent relocking process. These concepts are resolved in the generalized velocity description in equation (A17) and the incorporation of τ_w (equation (A18)) to the athermal strength τ_A in equation (A17) (see also equation (22)).

Strictly speaking, both $\rho_{mK}v_K$ and $\rho_{mw}v_w$ are always interconnected. The multiplication processes driven by the MK motion ($\rho_{mK}v_K$) or KWL unlocking ($\rho_{mw}v_w$) always result in a fresh set of the locked screw-character dislocations (KWLs) connected by a fresh set of MKs. We believe that an argument about whether or not these two contributions are separable is of little significance. It is

only important to understand that one mechanism can dominate over the other for the progress of plastic flow, depending on the level of the applied stress and the temperature. For instance, locking of screw-character dislocations tends to be so rapid that their contribution to plastic flow is less significant unless the applied stress becomes high enough to athermally unlock KWLs. This is the regime over which MK motion contributes significantly to plastic flow, whereas at higher stresses the motion of unlocked screw-character dislocations is the dominant mechanism.

4. Simulation outline

The constitutive formulations described in previous sections were used to predict the flow behaviour of Ni_3(Al,0.25%Hf) single crystals over a temperature range from 300 K to 1100 K for three different loading orientations in both tension and compression at a strain rate of 5×10^{-5}/sec. All constitutive formulations were implemented into the finite element software ABAQUS through a User MATerial subroutine (UMAT). A tangent modulus method [48] was used for the time integration. Preliminary parametric studies were performed in order to identify the physical nature and reasonable ranges for the values of the major input parameters that were used in the current constitutive formulations. Input parameters can be categorized into temperature-dependent and -independent parameters, and further into adjustable (*ad-hoc*) parameters and non-adjustable parameters that were determined from chemistry and physical property measurements. The elastic constants of Ni_3(Al,0.25%Hf) and their temperature dependence were determined by fitting Neveu's data for RT elastic constants of Ni_3(Al,0.25%H_f) [49] to Yoo's data for the temperature dependence of elastic constants of Ni_3Al [50]. The anisotropy factor A, energy factor K (hence μ) and their temperature dependence were determined from the elastic constants. The values of other major temperature-dependent input parameters are summarized in Table 1.

[Insert table 1 about here]

The CRSS for the octahedral slip system ($\tau_{o(oct)}$) was set to 33 MPa at 300 K and to decrease with temperature rise by 0.8 MPa per an increment of 100 K. The temperature dependence of CRSS for the cubic slip system ($\tau_{o(cubic)}$) followed the data from Allan [51]. The initial decay rate for the critical MK height (θ_{hc} in equation (7)) was set as 1.35 μm (per strain) at 300 K and assumed to linearly increase (0.19 μm/100K) with increasing temperature. The threshold stress (τ_i) for athermal unlocking of incomplete KWLs ($w \approx b$) was determined based on equation (1). The stress (τ_w^*) for athermal unlocking of KWLs having $w = \overline{w} + b$ was set to have a similar temperature dependence with τ_i (refer to [16] for details about τ_w^*). The temperature dependence of h_{co} and h_{cs} was determined from equations (9) and (10), respectively, and is plotted in figure 1. Both quantities were found to mildly decrease with increasing temperature.

[Insert figure 1 about here]

Other input parameters were divided into three groups, the ones tied to $\rho_{mK}v_K$, $\rho_{mw}v_w$, and parameters related with cubic slip, respectively, and are summarized in Table 2. A constant total MK density ($\rho_{Ktot} = 1.6\times10^{12}/\text{m}^2$ in equation (5)) was assumed for the current simulations. The initial decay rate for $\overline{h}$ ($\theta_{\overline{h}}$) was also set as a constant throughout the deformation and the magnitude of $\overline{h}_s$ was determined by setting a constant difference between $\overline{h}_o$ and $\overline{h}_s$ ($\overline{h}_o - \overline{h}_s = 60$ Å), after the magnitude of $\overline{h}_o$ was calculated from equation (11). The mobile screw-character dislocation density (ρ_{mw}) due to athermal unlocking of KWLs was assumed to be 4×10^{12} /m^2, which is comparable to experimental data for screw-character dislocation densities of Ni_3(Al,Hf,B) measured by Ezz et al. [32]. From the parametric study it was found that the magnitude of the 0.2% offset strength is influenced by the values of h_{co}, $\overline{h}_o$ (hence c_f and k_d in

equation (11)), ρ_{Ktot} and ρ_{mw}, while the SHR after the microstrain regime (> 0.5% ~ 1% strain) tends to depend mostly on the values of h_{cs}, $\bar{h}_s$, θ_{hc}, $\theta_{\bar{h}}$, θ_{10} and τ_w^*.

[Insert table 2 about here]

5. Simulation results and discussion

Simulated temperature dependences of [$\bar{1}$ 2 3]-compression flow stresses at different offset strains from 0.001% to 0.5% are plotted in figure 2 along with experiment 0.2%-offset data for [$\bar{1}$ 2 3] compression of Ni_3(Al,0.25%Hf) from Shi [52]. The simulation results captured general trends of the flow-stress anomaly for this alloy class. The flow stress was almost independent of temperature at extremely small offset strains (0.001% offset for the current case) [53]. However, the flow-stress anomaly was significant at higher offset strains (0.1% to 0.6% strains in figure 2). In particular, 0.2%-offset stresses exhibited a quantitative agreement in temperature dependence with those from Shi's data [52]. The simulation result indicated that the formation of the peak stress at about 1000 K was related with the activation of cubic slip systems. After 900 K, the CRSS for cubic slip that was adopted from Allan's data [25] rapidly dropped to 285 MPa for 1000 K and to 220 MPa for 1100 K (Table 1). This is believed to facilitate the activation of cubic slip at high temperatures (see figure 5).

[Insert figure 2 about here]

Figure 3 shows the temperature dependence of normalized SHRs measured at 0.9% axial strain ($\varepsilon_{[\bar{1}23]}$) from simulated compression flow curves for the [$\bar{1}$ 2 3] orientation. Experimental SHR data measured at 2% shear strain ($\gamma_{(111)[10\bar{1}]}$) for Ni_3(Al,0.25%Hf) [52] are also plotted in this

figure for comparison. The simulation result well captured the detailed temperature dependence observed in the experimental data. Both predicted and experimental SHRs peaked around 700 K ~ 800 K and decreased over the range 800 K ~ 900 K. However, a discrepancy between simulation and experimental results was found at around 1100 K in figure 3. The simulation predicted the monotonic decrease in SHR even after 900 K, which contradicted the experimental observations. This is probably because 1100 K is above the positive temperature-dependent flow-stress regime (referred to as domain B by Veyssière and Saada [30]), and the framework of the present constitutive model may not completely cover detailed mechanisms that are feasible at such a high temperature range.

[Insert figure 3 about here]

Formation of the SHR peak in the simulation turned out to be closely related with the initiation of athermal unlocking of incomplete KWLs, which indicates that v_w in equations (22) and (A17) becomes active as the applied stress τ is larger than the stress τ_i to unlock the weakest incomplete KWLs. The relative contribution of screw-dislocation motion is shown more clearly in Figure 4, which plots the volume-averaged shear rate for the screw segments (the second term of the RHS of equation (3) *viz.*, $\dot{\gamma}_w = b\rho_{mw}v_w$), with the axial strain for [$\bar{1}$ 2 3] compression at temperatures of 600 K, 700 K and 800 K. Here, one can see the initiation (or activation) of $\dot{\gamma}_w$ at around 0.7% strain for 800 K and around 1.4% strain for 700 K, which led to the decrease in SHR (for 0.9% strain) after the peak at between 700 K and 800 K, as seen in figure 3. This result is consistent with the peak SHR-KWL unlocking relation suggested by Caillard [34] and by Kruml et al. [35].

[Insert figure 4 about here]

The simulated axial stress - axial strain curves for [$\bar{1}$ 2 3] compression are plotted in figure 5 for high temperatures from 800 K to 1100 K. Here, two solid arrows indicate the points at which

cubic slip is initiated for simulated stress - strain curves at 1000 K and 1100 K, respectively. In figure 5, all simulated flow curves showed 'indistinguishably smooth' elastic-to-plastic transition that is typical for Ni_3Al-based single crystals at elevated temperatures: the onset of plastic flow is indicated by a broken arrow in figure 5. In a strain range between the onset of plastic flow and the initiation of $\dot{\gamma}_w$ or cubic slip (usually less than 0.5% ~ 1% axial strain), simulated flow curves showed increasing SHR with increasing temperature from 800 K to 1000 K. This stems from the strong temperature-dependence of $\dot{\gamma}_K$ ($= b\rho_{mK}v_k$ in equation (3)) through ρ_{mK} (equation (5)), which was described as 'source-controlled plastic flow' and its temperature dependence in section 3.3. However, one may notice that the simulated SHR tends to decrease upon activation of cubic slip, as indicated by arrows for 1000 K and 1100 K.

[Insert figure 5 about here]

The simulation results suggest that the competitive (or selective) initiation of $\dot{\gamma}_w$ and cubic slip influences the SHR variation with temperature in figure 3. However, whether or not this explanation is applicable to understanding the SHR variation around 1100 K is still unknown, because the current constitutive model does not treat the hardening behaviour of cubic slip in an accurate way. This was due to the lack of information on the cubic-slip behaviour for Ni_3Al-based single crystals. Nevertheless, we are convinced from the simulation results that the temperature dependence of the SHRs varies dramatically with accumulated strain. This SHR variation seems to be particularly noticeable in the small-strain regime (≤ 1% ~ 3%) where the selective initiation of different plastic-flow mechanisms is expected to occur. Figure 6 demonstrates the influence of accumulated strain on the observation of the anomalous SHR behaviour, which shows the SHR at two levels of strain (0.9% and 3%) plotted as a function of temperature for [$\bar{1}$ 2 3] compression (hence the curve for SHR at 0.9% strain in figure 6 is the

same simulation result as shown in figure 3). In figure 6, the peak-SHR temperature decreased to 600 K from 700 K ~ 800 K with increasing levels of strain. Therefore, any correlation between the anomalous temperature-dependent SHR behavior (e.g. formation of a peak) and the onset of a particular dislocation mechanism must consider whether the accumulated strain at which the SHRs are determined is within the range that the intended flow mechanism is expected to be active.

[Insert figure 6 about here]

Simulations were also performed for tension and compression in three different loading directions, [$\bar{1}$ 2 3], N[$\bar{1}$ 1 1] (which is just 5 degrees off from the [$\bar{1}$ 1 1] direction) and [$\bar{1}$ 2 12] (which is 10 degrees off from the [$\bar{1}$ 0 0] direction). As stated in the previous section the T-C asymmetric behaviour is controlled by equation (14) (particularly by κ and κ') in the present model. Figure 7 shows the resulting 0.2%-offset flow stress versus temperature curves for the three different orientations and two loading conditions. The simulation results captured the general trend of the T-C asymmetric behaviour of Ni_3Al-based single crystals. The N[$\bar{1}$ 1 1]-oriented simulation exhibited the largest T-C difference at the peak temperature (1000 K). The absolute magnitude of the T-C difference for the N[$\bar{1}$ 1 1] and [$\bar{1}$ 2 12] orientations is almost identical in the anomalous temperature regime. However, unlike the [$\bar{1}$ 2 3] and [$\bar{1}$ 1 1] orientations, the flow stress in tension was higher than that in compression for [$\bar{1}$ 1 12] simulation. The simulated peak temperature ($T_p(\tau_{0.2\%})$) for the 0.2%-offset flow stress was also found be loading-orientation dependent. The present simulation showed $T_p(\tau_{0.2\%})$'s at about 900 K, 1000 K and above 1000 K for N[$\bar{1}$ 1 1], [$\bar{1}$ 2 3] and [$\bar{1}$ 2 12] loading, respectively. All these qualitative T-C asymmetry trends are typical for Ni_3Al-based single crystals [54-56].

[Insert figure 7 about here]

6. Concluding remarks

We have shown that a new constitutive model is capable of capturing many of the major thermo-mechanical features of Ni_3Al-based $L1_2$ intermetallic single crystals. One of the significant results from the present simulations is that anomalous flow features of Ni_3Al-based single crystals can be predicted by monitoring the density of three populations of mobile dislocations—macro-kinks, athermally-unlocked screw-character dislocations on the octahedral planes, and dislocations gliding on cubic planes. Using this formalism, the limited release (or mobilization) of MKs turned out to play a key role in controlling plastic flow for the situation where all screw-character dislocations are locked to form KWLs, hence controlling the flow stress and the consequent SHR. This situation is expected over the micro-strain regime including the onset of plastic flow where 'effectively' instantaneous locking of screw-character dislocations dominates and the 'smooth' elastic-plastic transition is observed in the flow curve. Since the formation of KWLs depends largely upon temperature, the distribution of MK heights and the MK mobilization are also influenced by temperature, and so is their influence on plastic flow. The present constitutive model represented this idea by formulating the mobilization (or release) of MKs based upon the distribution of MK heights. That representation also included the evolution of MK heights with strain and temperature through a thermally activated cross-slip-locking process, and incorporated this evolution into the corresponding mobile density and plastic strain rate.

In the present constitutive model, the formulation of the threshold stress τ_i for athermal unlocking of incomplete KWLs ($w \approx b$) was adopted directly from that suggested by Caillard and Paidar

[34,36]. This stress was used as a saturation stress for setting the limiting minimum active MK height. For the current simulation τ_i ranged between 255 MPa and 247 MPa in a temperature range from 300 K to 1100 K, as shown in Table 1. However, a disparity was found between τ_i for the current simulation (i.e. Caillard) and the KWL-unlocking stress (τ_u) adopted by Devincre and Veyssière et al. for their DD simulations [20], which was given by $\tau_u(w) = 16.5(w/b) + 50$ (MPa) [57] *viz.*, $\tau_u = 66.5$ MPa for $w = b$. If the present model were to use τ_u instead of τ_i for unlocking of incomplete KWLs, one would see results that are quite different from those obtained by the current simulations. Our previous constitutive model [28] that utilized Caillard's exhaustion hardening model [16] set the KWL-unlocking stress to have a magnitude comparable with τ_u from Devincre and Veyssière et al. These simulations were able to accurately represent the flow-stress anomalies (figure 1 in [28]). However, that model failed to capture the salient details in the temperature dependence of SHRs (figure 2 in [28]).

We have been successful in modeling the anomalous temperature dependence of the SHR by introducing the selective initiation of different types of plastic flow mechanisms (both $\dot{\gamma}_w$ and cubic slip for the current simulation). However, this does not guarantee that our interpretation of the present modeling results is physically applicable to the actual flow behaviour. Importantly, these results can be used to point out deficiencies in the current understanding of the deformation behaviour in $L1_2$ alloys, and guide future experimental work. We believe that the present model will be more reliable if the flow behaviour of cubic slip (particularly the mobility of edge-, screw- and mixed-character dislocations on the cubic plane and the temperature dependence of their gliding behaviour) is better implemented based upon an empirically-verified understanding.

Acknowledgements

The present work was supported by the U.S. Defense Advanced Research Projects Agency and the Air Force Office of Scientific Research. YSC and TAP acknowledge support from the Materials and Manufacturing Directorate under contract #'s F33615-96-C-5258 and F33615-01-5214. The authors acknowledge fruitful discussion with Drs. S. Rao, UES, Inc, and C. Woodward, AFRL/MLLM. The computations described in this study were performed using computer resources at the Ohio Supercomputer Centre (grant #'s PAS0191 and PAS0647) with the collaboration of Professors S. Ghosh and G. Daehn of The Ohio State University.

Appendix A: Summary of constitutive formulations

For octahedral slip systems,

$$\dot{\gamma}^s = b(\rho^s_{mK} v^s_K + \rho^s_{mw} v^s_w) \cdot sign(\tau^s) \tag{A1}$$

$$v^s_K = \frac{\left|\tau^s\right| - \tau^s_K}{B} b \tag{A2}$$

$$\tau^s_K = \tau_o + \tau^s_f \tag{A3}$$

$$\frac{d\tau^s_f}{d\gamma} = \theta_f \left(\frac{\tau_{fs} - \tau^s_f}{\tau_{fs}} \right) \tag{A4}$$

$$\rho^s_{mK} = \rho_{Ktot} \cdot f^s_{mK}(\gamma, T) \tag{A5}$$

$$f^s_{mK} = \exp\left(-\frac{h^s_c}{\bar{h}^s} \right) \tag{A6}$$

$$\frac{dh^s_c}{d\gamma} = -\theta_{hc} \left(\frac{h^s_c - h_{cs}}{h_{co} - h_{cs}} \right) \tag{A7}$$

$$\frac{d\bar{h}^s}{d\gamma} = -\theta_{\bar{h}} \left(\frac{\bar{h}^s - \bar{h}_s}{\bar{h}_o - \bar{h}_s} \right) \tag{A8}$$

$$h_{co}(T) = \frac{\alpha \mu(T) b}{\tau_o(T)} \tag{A9}$$

$$h_{cs}(T) = \frac{\alpha \mu(T) b}{\tau_i(T)} \tag{A10}$$

$$\bar{h}^s_o(T) = c_f \exp\left(\frac{k_d G^s_{KPo}}{kT} \right) \tag{A11}$$

$$\tau_i = \frac{\Gamma_{111}}{b} \left(1 - \frac{\Gamma_{010}}{\Gamma_{111}} \frac{1 + 2/A}{\sqrt{3}} \right) \tag{A12}$$

$$G_{KP}^{s} = 2U_{c}^{s} + Kb^{3}\left[2\sqrt{2\alpha' r} - \sqrt{\frac{\tau_{cs}^{s}}{2\pi K}}\right] \tag{A13}$$

$$U_{c}^{s} = \frac{\mu b^{3}}{4\pi} h' + \frac{\mu b^{3}}{4\pi} \kappa' \frac{b}{\Gamma_{111}} \left[\tau_{pe}^{s} - \kappa \tau_{se}^{s}\right] \frac{\Gamma_{111}}{\Gamma_{CSF}} \tag{A14}$$

$$\tau_{CS}^{s} = \frac{\Gamma_{111}}{b}\left[\frac{A\sqrt{3}}{A+2} - \frac{\Gamma_{100}}{\Gamma_{111}}\right] + \tau_{cb}^{s} \tag{A15}$$

$$\frac{d\rho_{mw}}{d\gamma} = 0 \tag{A16}$$

$$v_{w}^{s} = v_{o} \exp\left(-\frac{F_{o}}{kT}\left[1 - \left[\frac{\left|\tau^{s}\right| - \tau_{w}^{s}}{\tau_{T}}\right]^{p}\right]^{q}\right) \quad \text{if } \tau^{s} > \tau_{i} \tag{A17}$$

$$\frac{d\tau_{w}^{s}}{d\gamma} = \theta_{10} \exp\left(-\frac{G_{CS}^{s}}{kT}\right) \exp\left(-\frac{\tau_{w}^{s} - \tau_{i}}{\tau_{w}^{*} - \tau_{i}}\right) \tag{A18}$$

$$G_{CS}^{s} = U_{c}^{s} + K^{2} b^{3}\left[\frac{4r\sqrt{2\alpha' r}}{3\tau_{cs}^{s}}\right] \tag{A19}$$

For cubic slip systems,

$$\dot{\gamma}^{s} = b\rho_{mc}^{s} v_{c}^{s} \cdot sign(\tau^{s}) \tag{A20}$$

$$v_{c}^{s} = v_{o} \exp\left(-\frac{F_{o(cubic)}}{kT}\left[1 - \left[\frac{\left|\tau^{s}\right| - \tau_{c}^{s}}{\tau_{T(cubic)}}\right]^{p_{c}}\right]^{q_{c}}\right) \quad \text{if } \tau^{s} > \tau_{o(cubic)} \tag{A21}$$

$$\tau_{c}^{s} = \tau_{o(cubic)} + \tau_{f(cubic)}^{s} \tag{A22}$$

$$\frac{d\tau_{f(cubic)}^{s}}{d\gamma} = \theta_{c}\left(\frac{\tau_{fs(cubic)} - \tau_{f(cubic)}^{s}}{\tau_{fs(cubic)}}\right) \tag{A23}$$

7. References

[1] M. Yamaguchi, V. Paidar and D.P. Pope, Phil. Mag. **18** 773 (1968).

[2] V. Paidar, M. Yamaguchi, D.P. Pope and V. Vitek, Phil. Mag A **45** 883 (1982).

[3] B.H. Kear and H.G.F. Wilsdorf, Trans. AIME **224** 382 (1962).

[4] B.H. Kear, Acta Metall. **12** 555 (1964).

[5] S. Takeuchi and E. Kuramoto, Acta Metall. **21** 415 (1973).

[6] C. Lall, S. Chin and D.P. Pope, Metall. Trans. A **10** 1323 (1979).

[7] V. Paidar, D.P. Pope and V. Vitek, Acta Metall. **32** 435 (1984).

[8] M.H. Yoo, Scripta Metall. **20** 915 (1986).

[9] M.J. Mills, N. Baluc and H.P. Karnthaler, in *High-Temperature Ordered Intermetallic Alloys III*, MRS Symp. Proc. Vol. 133, edited by C.C. Kock, C.T. Liu, N.S. Stoloff and A.I. Taub (MRS, Pittsgurgh, PA, 1989), pp. 203.

[10] Y.Q. Sun and P.M. Hazzledine, Phil. Mag. A **58** 603 (1988).

[11] P.B. Hirsch, Phil. Mag. A **65** 569 (1992).

[12] P.B. Hirsch, Prog. Mat. Sci. **36** 63 (1992).

[13] S.S. Ezz and P.B. Hirsch, Phil. Mag. A **69** 105 (1994).

[14] S.S. Ezz and P.B. Hirsch, Phil. Mag. A **72** 383 (1995).

[15] S.S. Ezz and P.B. Hirsch, Phil. Mag. A **73** 1069 (1996).

[16] D. Caillard, Acta Mater. **44** 2773 (1996).

[17] F. Louchet, Mat. Sci. Eng. A **234-236** 275 (1997).

[18] M.J. Mills and D.C. Chrzan, Acta Metall. Mater. **40** 3051 (1992).

[19] B. Devincre, P. Veyssière, L.P. Kubin and G. Saada, Phil. Mag. A **75** 1263 (1997).

[20] B. Devincre, P. Veyssière and G. Saada, Phil. Mag. A **79** 1609 (1999).

[21] Q. Qin and J.L. Bassani, J. Mech. Phys. Sol. **40** 813 (1992).

[22] Q. Qin, J.L. Bassani, J. Mech. Phys. Sol. **40** 835 (1992).

[23] A.M. Quitino and M. Ortiz, Mat. Sci. Eng A **170** 111 (1993).

[24] V. Vitek, D.P. Pope and J.L. Bassani, in *Dislocations in Solids*, Vol. 10, edited by F.R.N. Nabarro and M.S. Duesbery (Elsevier, New York, 1996), Chapter 51.

[25] C.D. Allan, Ph.D. Thesis, MIT (1995).

[26] T. Kameda and M.A. Zikry, Scripta Mater. **38** 631 (1998).

[27] Y. Yuan and D.M. Parks, paper presented at the 2nd Int. Conf. on Multiscale Materials Modeling (MMM-II), Los Angeles, CA, 11-15 Oct. (2004).

[28] Y.S. Choi, D.M. Dimiduk, M.D. Uchic and T.A Parthasarathy, Mat. Sci. Eng. A **400-401** 256 (2005).

[29] P.B. Hirsch, in *Dislocations in Solids*, Vol. 11, edited by F.R.N. Nabarro and M.S. Duesbery (Elsevier, New York, 2002), Commentary pp. xxv.

[30] P. Veyssière and G. Saada, in *Dislocations in Solids*, Vol. 10, edited by F.R.N. Nabarro and M.S. Duesbery (Elsevier, New York, 1996), Chapter 53.

[31] D. Caillard, G. Molénat and V. Paidar, Mat. Sci. Eng. A **234-236** 695 (1997).

[32] S.S. Ezz, Y.Q. Sun and P.B. Hirsch, Mat. Sci. Eng. A **192-193** 45 (1995).

[33] S.S. Ezz, Acta Mater. **44** 4395 (1996).

[34] D. Caillard, Mat. Sci. Eng. A **319-321** 74 (2001).

[35] T. Kruml, E. Conforto, B. Lo Piccolo, D. Caillard and J.L. Martin, Acta Mater. **50** 5091 (2002).

[36] D. Caillard and V. Paidar, Acta Mater. **44** 2759 (1996).

[37] E. Conforto, G. Molénat and D. Caillard, Phil. Mag. A **85** 117 (2005).

[38] E. Orowan, Phil. Trans. Roy. Soc. London A **52** 8 (1940).

[39] A. Arsenlis and D.M. Parks, J. Mech. Phys. Sol. **50** 1979 (2002).

[40] K.-S. Cheong and E.P. Busso, Acta Mater. **52** 5665 (2004).

[41] E. Nadgorny, Prog. Mat. Sci. **31** 1 (1988).

[42] A Couret, Y.Q. Sun and P.M. Hazzledine, in *High-Temperature Ordered Intermetallic Alloys IV*, MRS Symp. Proc. Vol. 213, edited by L.A. Johnson, D.P. Pope and J.O. Stiegler (MRS, Pittsgurgh, PA, 1991), pp. 317.

[43] A. Couret, Y.Q. Sun and P.B. Hirsch, Phil. Mag. A **67** 29 (1993).

[44] J.P. Hirth and J. Lothe, *Theory of Dislocations* (Wiley-Interscience Publication, New York, 1982).

[45] M.H. Yoo, J.A. Horton and C.T. Liu, Acta Metall. **36** 2935 (1988).

[46] U.F. Kocks, A.S. Argon and M.F. Ashby, Prog. Mat. Sci. **19** 1 (1975).

[47] S. Balasubramanian and L. Anand, J. Mech. Phys. Sol. **50** 101 (2002).

[48] D. Peirce, R.J. Asaro and A. Needleman, Acta Metall. **31** 1951 (1983).

[49] C. Neveu, Thèse de Doctorat, l'Université Paris-Sud Centre d'ORSAY, France (1995).

[50] M.H. Yoo, Acta Metall. **35** 1559 (1987).

[51] C.D. Allan, Ph.D. Thesis, MIT, USA (1995).

[52] X. Shi, Thèse de Doctorat, l'Université Paris-Nord, France (1995).

[53] P.H. Thornton, R.G. Davies and T.L. Johnston, Metall. Trans. **1** 207 (1970).

[54] S.S. Ezz, D.P. Pope and V. Paidar, Acta Metall. **30** 921 (1982).

[55] F.E. Heredia and D.P. Pope, Acta Metall. Mater. **39** 2027 (1991).

[56] Y. Umakoshi, D.P. Pope and V. Vitek, Acta Metall. **32** 449 (1984).

[57] G. Saada and P. Veyssière, Phil. Mag. A **70** 925 (1994).

[58] D.M. Dimiduk, J. de Physique III **1** 1025 (1991).

[59] Y.S. Choi, D.M. Dimiduk, M.D. Uchic and T.A Parthasarathy, Phil. Mag. Manuscript In Preparation (2006).

Table 1. Major temperature-dependent input parameters

	300 K	400 K	500 K	600 K	700 K	800 K	900 K	1000 K	1100 K
A	3.282	3.308	3.336	3.365	3.395	3.427	3.462	3.499	3.539
K (GPa)	70.7	69.0	67.3	65.5	63.7	61.7	59.7	57.6	55.4
$\tau_{o(\mathrm{oct})}$ (MPa)	33	32.2	31.4	30.6	29.8	29	28.2	27.4	26.6
$\tau_{o(\mathrm{cubic})}$ (MPa)	350	350	350	350	350	350	350	285	220
θ_{hc} (μm)	1.35	1.54	1.73	1.92	2.11	2.30	2.49	2.68	2.87
τ_i (MPa)	255	254	253	252	251	250	249	248	247
τ_w^* (MPa)	265	264	263	267	271	275	279	283	287
θ_{10} (GPa)	10	15	20	25	30	35	40	40	40

Table 2. Input parameters used for the current simulations

ρ_{mK} and v_K		ρ_{mw} and v_w		Cubic slip	
B	0.002 Pa	ρ_{mw}	4×10^{12} /m^2	ρ_{mc}	4×10^{12} /m^2
θ_f	300 MPa	v_o	1 /sec	$F_{o(cubic)}$	6×10^{-19} J
τ_{fs}	200 MPa	F_o	3×10^{-19} J	p_c	3/4
ρ_{Ktot}	1.6×10^{12} /m^2	τ_T	20 MPa	q_c	3/2
$\theta_{\bar{h}}$	1600 Å	p	1/2	$\tau_{T(cubic)}$	200 MPa
$\bar{h}_o - \bar{h}_s$	60 Å	q	3/2	$\theta_{f(cubic)}$	100 MPa
α	1/3	h'	0.083	$\tau_{fs(cubic)}$	100 MPa
c_f	83 Å	κ'	-0.4		
k_d	0.11	κ	0.3		
α'	0.1	Γ_{111}	0.25 J/m^2		
r	0.001	Γ_{100}	0.20 J/m^2		
b	2.52 Å	Γ_{CSF}	0.32 J/m^2		

<List of Figures>

Figure 6. Normalized SHRs-temperature plots measured at 0.9% and 3% strains from simulated compression flow curves for a [-1 2 3] orientation.

Figure 7. Simulated 0.2%-offset flow-stress anomaly plots for tension and compression in the [-1 2 3] (squares), N[-1 1 1] (triangles) and [-1 2 12] (circles) crystallographic directions. Closed marks with a solid connecting line and open marks with a dashed line indicate compression and tension loading, respectively.

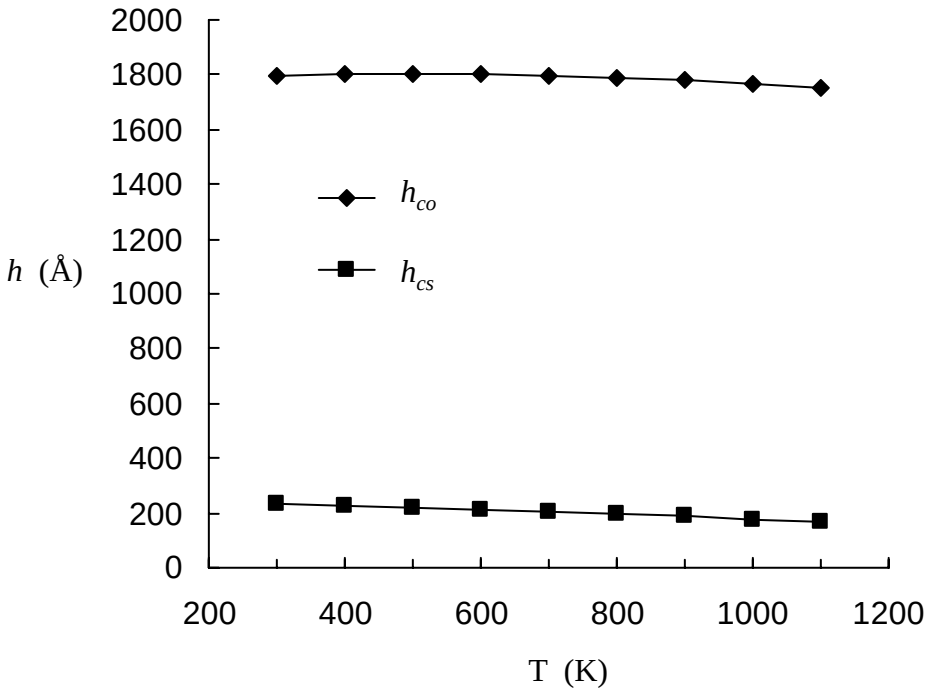
2000
1800
1600
1400
1200
1000
800
600
400
200
0
h (Å)
h_{co}
h_{cs}
200
400
600
800
1000
1200
T (K)

Figure 1

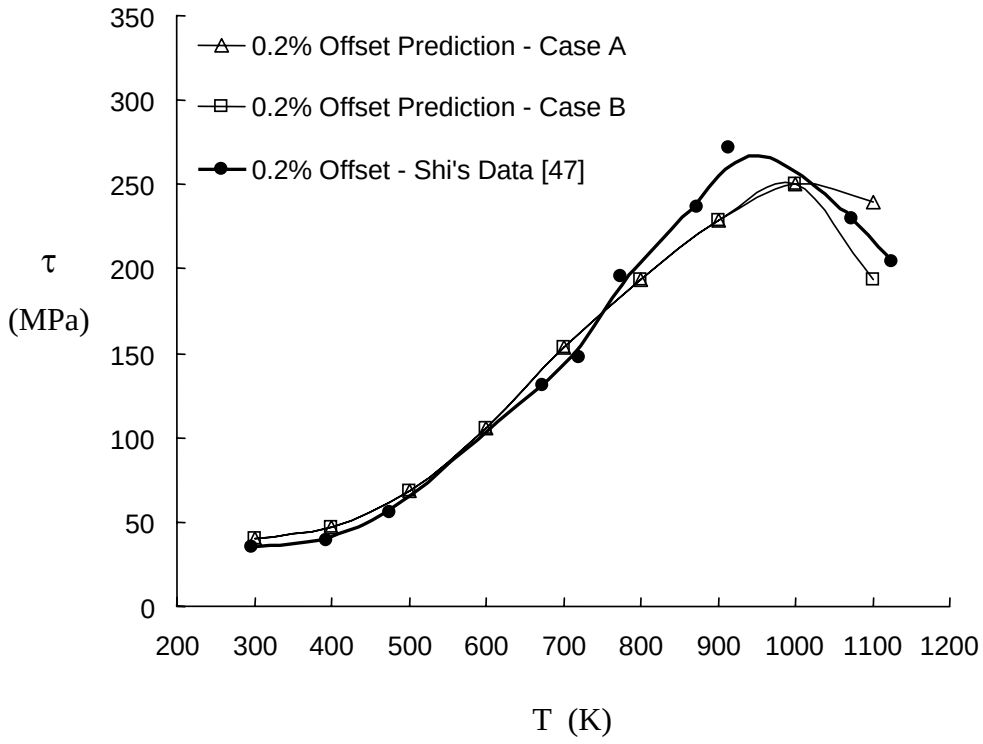
0.2% Offset Prediction - Case A
0.2% Offset Prediction - Case B
0.2% Offset - Shi's Data [47]
τ
(MPa)
350
300
250
200
150
100
50
0
200
300
400
500
600
700
800
900
1000
1100
1200
T (K)

Figure 2

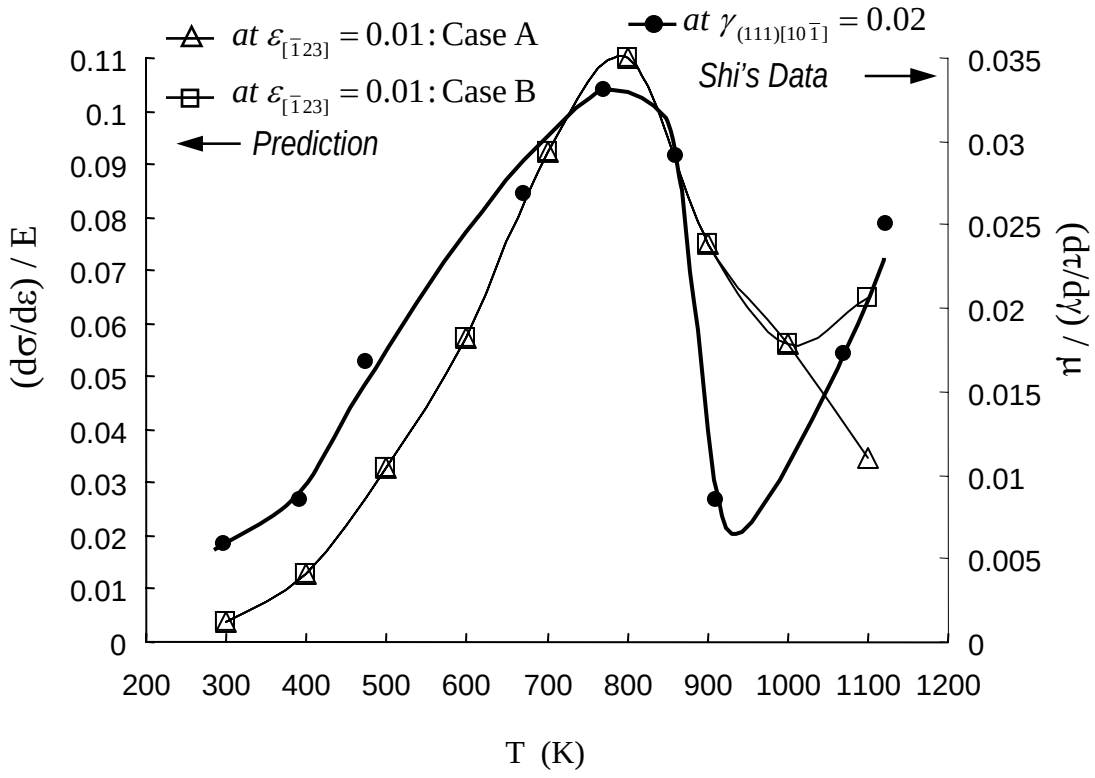
at $\varepsilon_{[\bar{1}\bar{1}23]} = 0.01$: Case A
at $\varepsilon_{[\bar{1}\bar{1}23]} = 0.01$: Case B
Prediction
at $\gamma_{(111)[10\bar{1}]} = 0.02$
Shi's Data
(dσ/dε) / E
dτ/dγ) / μ
T (K)
0.11
0.1
0.09
0.08
0.07
0.06
0.05
0.04
0.03
0.02
0.01
0
0.035
0.03
0.025
0.02
0.015
0.01
0.005
0
200
300
400
500
600
700
800
900
1000
1100
1200

Figure 3

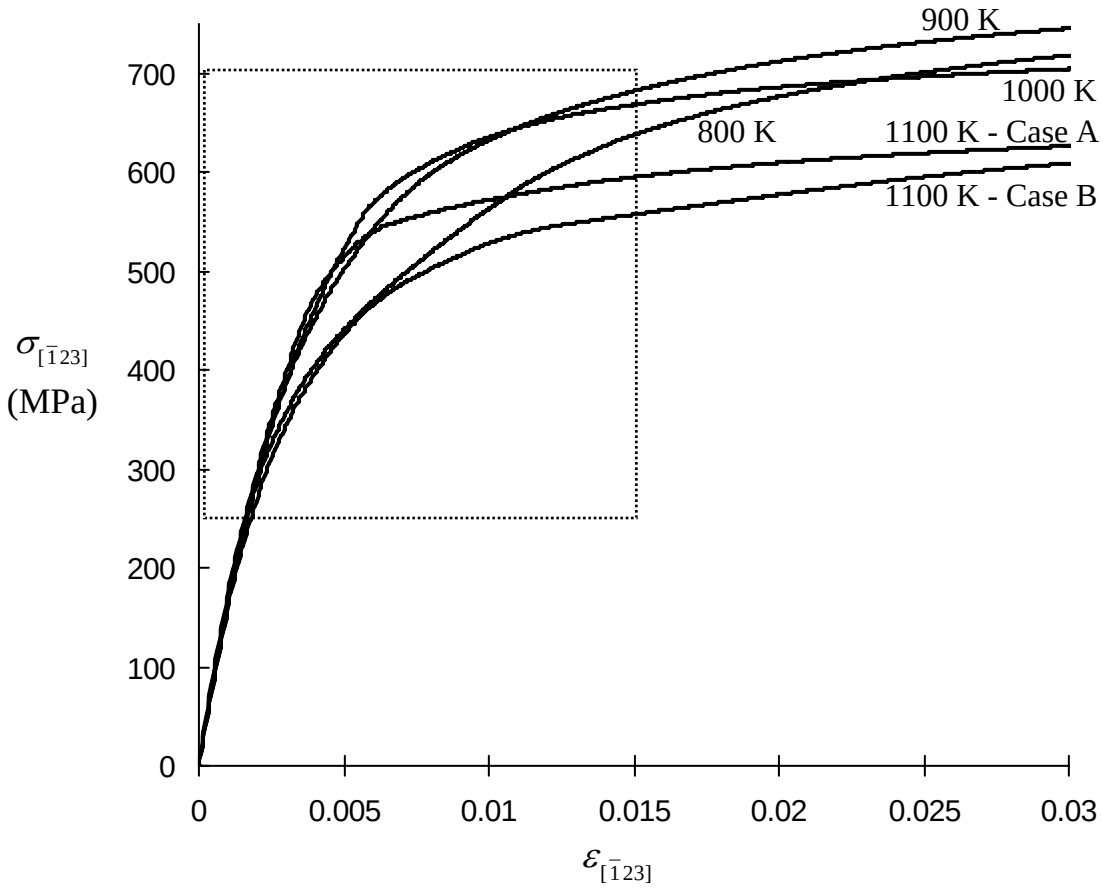
900 K
1000 K
800 K
1100 K - Case A
1100 K - Case B
700
600
500
400
300
200
100
0
$\sigma_{[\bar{1}23]}$
(MPa)
0
0.005
0.01
0.015
0.02
0.025
0.03
$\varepsilon_{[\bar{1}23]}$

Figure 4

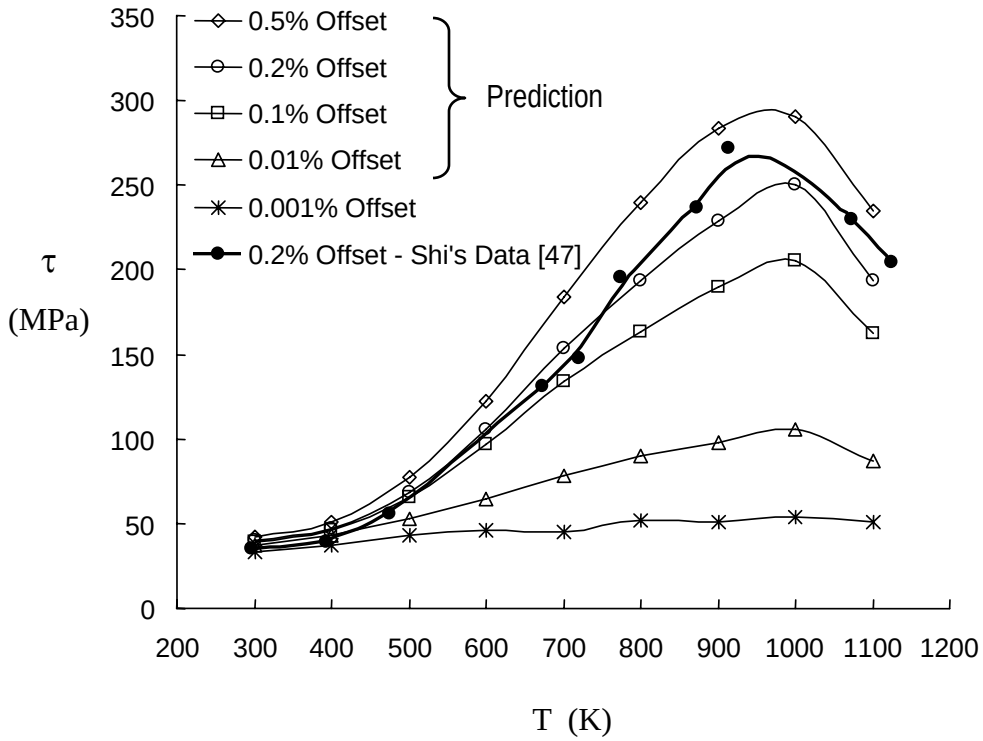
0.5% Offset
0.2% Offset
0.1% Offset
0.01% Offset
0.001% Offset
0.2% Offset - Shi's Data [47]
Prediction
τ
(MPa)
350
300
250
200
150
100
50
0
200
300
400
500
600
700
800
900
1000
1100
1200
T (K)

Figure 5

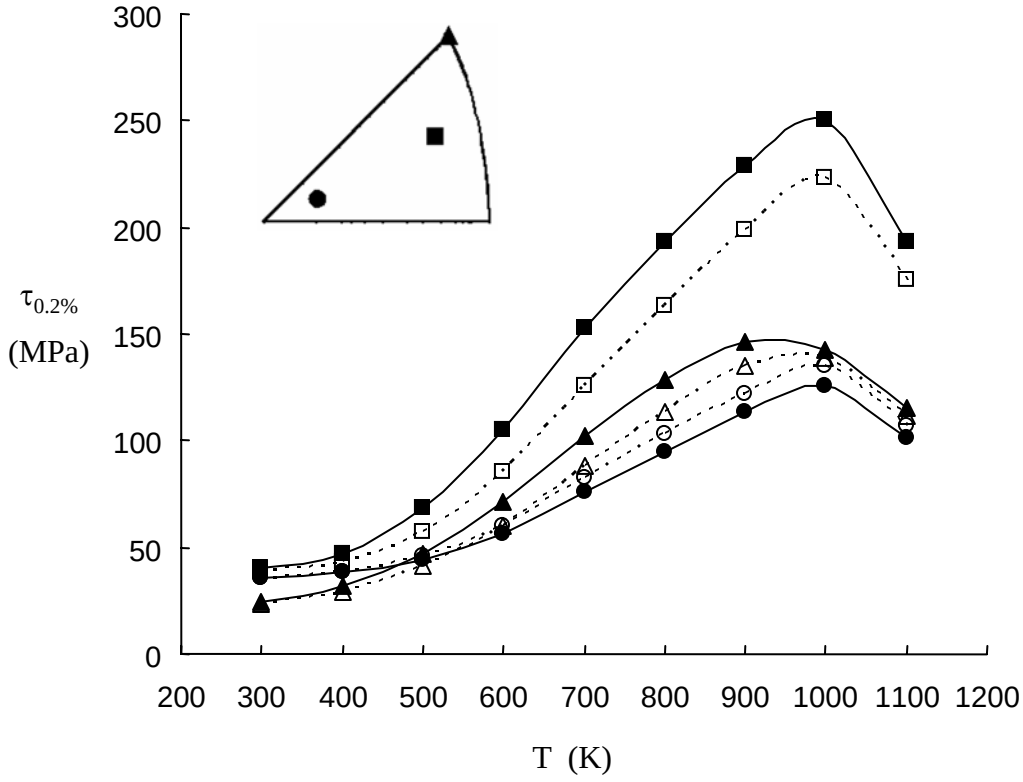
300
250
200
150
100
50
0
$\tau_{0.2\%}$
(MPa)
200
300
400
500
600
700
800
900
1000
1100
1200
T (K)

Figure 6

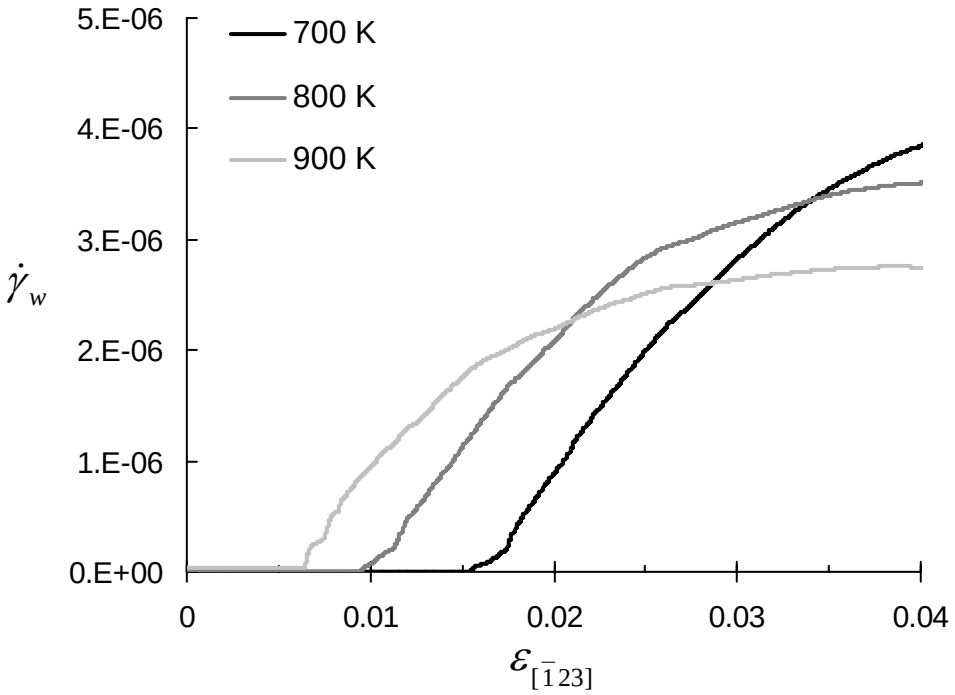
5.E-06
4.E-06
3.E-06
2.E-06
1.E-06
0.E+00
700 K
800 K
900 K
$\dot{\gamma}_w$
0
0.01
0.02
0.03
0.04
$\varepsilon_{[\bar{1}23]}$

Figure 7

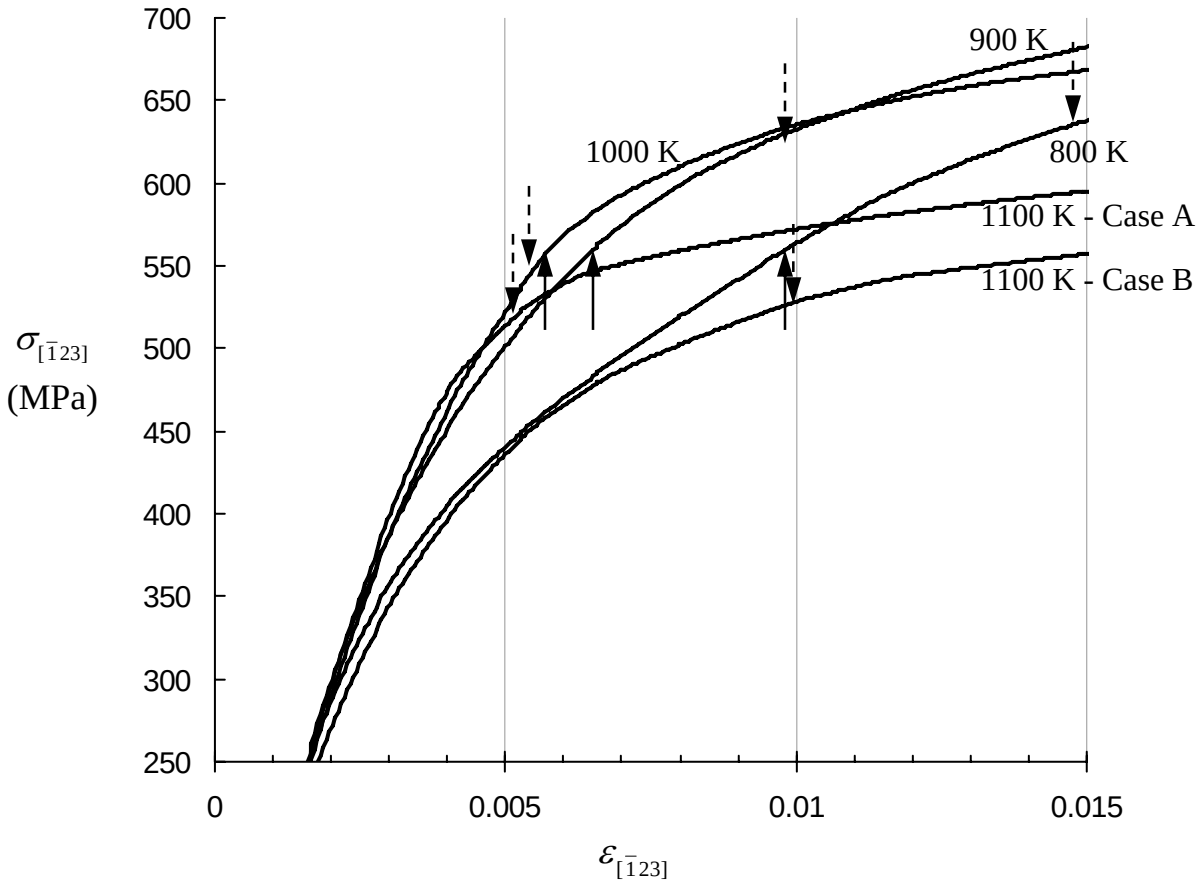
700
650
600
550
500
450
400
350
300
250
0
0.005
0.01
0.015
900 K
1000 K
800 K
1100 K - Case A
1100 K - Case B
$\sigma_{[\bar{1}23]}$
(MPa)
$\varepsilon_{[\bar{1}23]}$

Figure 8

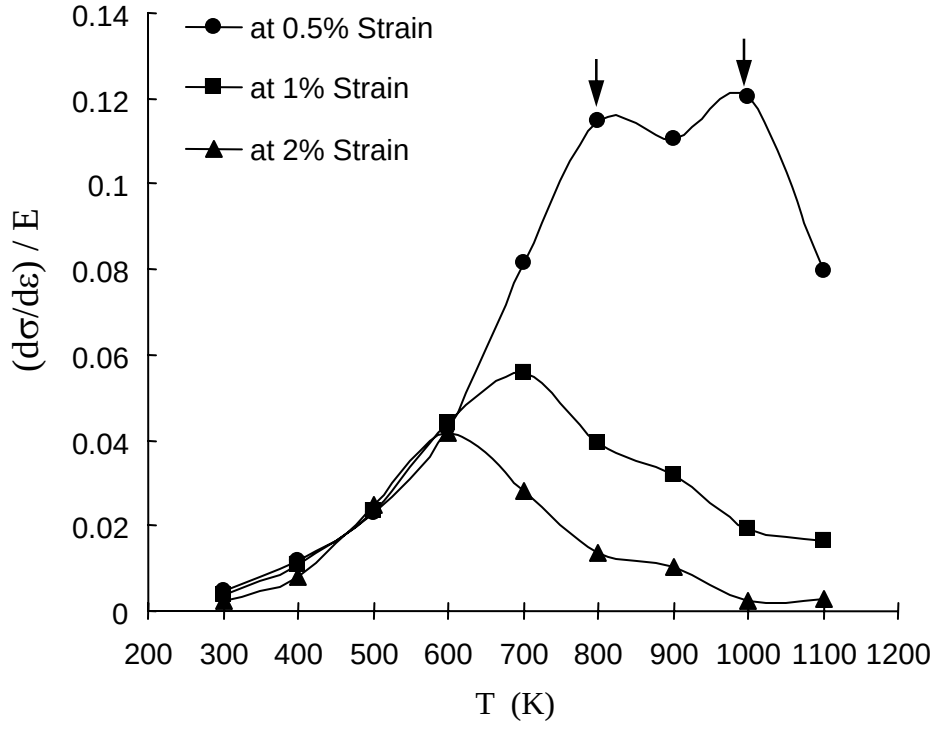
0.14
0.12
0.1
0.08
0.06
0.04
0.02
0
(dσ/dε) / E
at 0.5% Strain
at 1% Strain
at 2% Strain
200
300
400
500
600
700
800
900
1000
1100
1200
T (K)

Figure 9

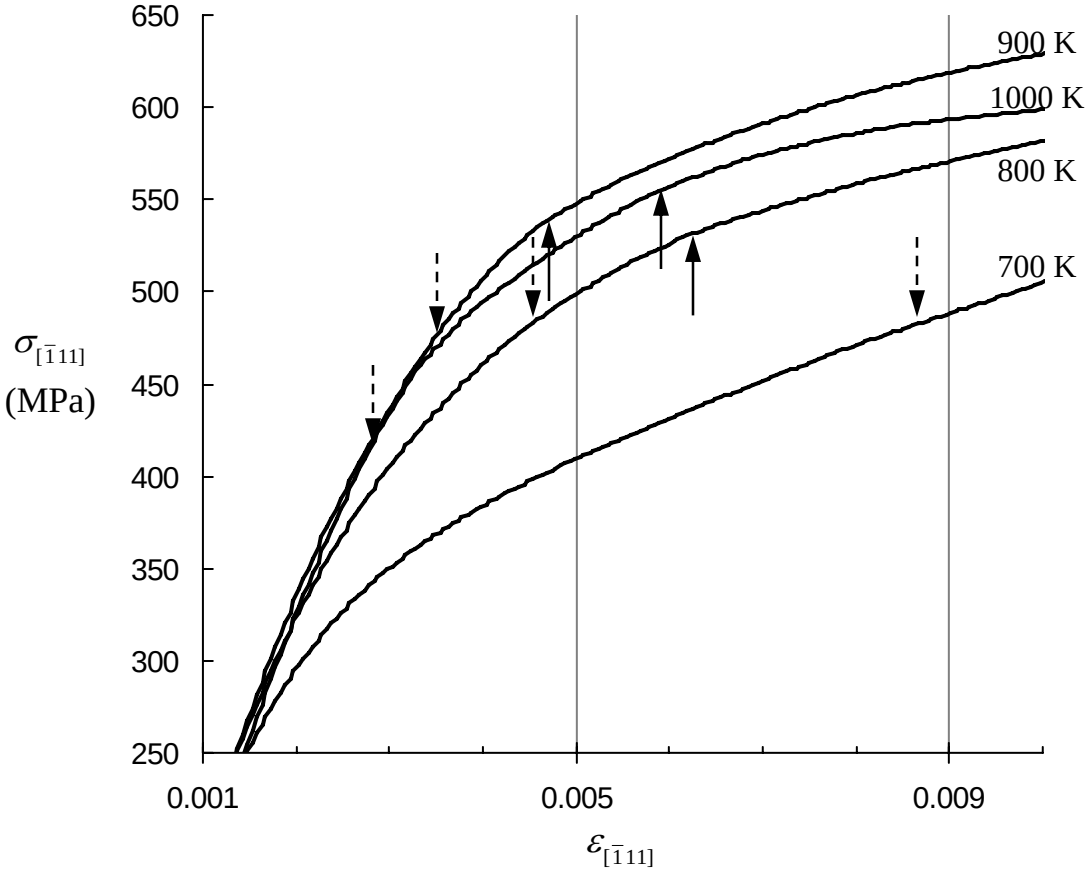
650
600
550
500
450
400
350
300
250
0.001
0.005
0.009
900 K
1000 K
800 K
700 K
$\sigma_{[\bar{1}11]}$
(MPa)
$\varepsilon_{[\bar{1}11]}$

Figure 10